Journal of Micromechanics and Microengineering

# Evolution of transient meniscus in a wettable microchannel for Newtonian fluid

To cite this article: Seung Mo Kim *et al* 2006 *J. Micromech. Microeng.* **16** 2692

View the article online for updates and enhancements.

You may also like

- Investigation of pulse voltage shape effects on electrohydrodynamic jets using a vision measurement technique
Kye-Si Kwon and Dae-Yong Lee
- Meniscus fabrication of halide perovskite thin films at high throughput for large area and low-cost solar panels
Xuezeng Dai, Yehao Deng, Charles H Van Brackle et al.
- A three-dimensional printed silk-based biomimetic tri-layered meniscus for potential patient-specific implantation
Ashutosh Bandyopadhyay and Biman B Mandal

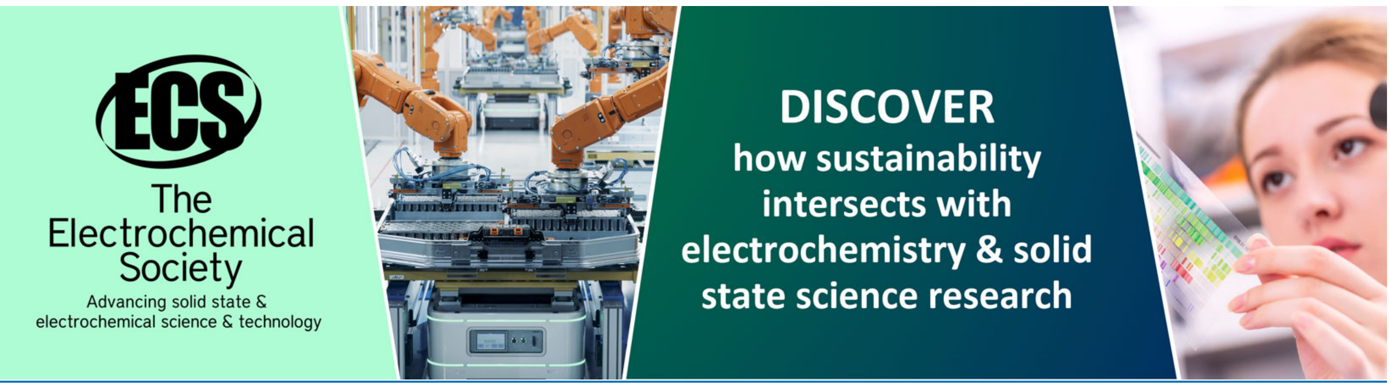


This content was downloaded from IP address 18.118.166.98 on 04/05/2024 at 17:07

J. Micromech. Microeng. **16** (2006) 2692–2696 doi:10.1088/0960-1317/16/12/023

# Evolution of transient meniscus in a wettable microchannel for Newtonian fluid

**Seung Mo Kim, Woo Il Lee and Kahp Y Suh**

School of Mechanical and Aerospace Engineering, Seoul National University, Seoul 151-742, Korea

E-mail: wilee@snu.ac.kr and sky4u@snu.ac.kr

Received 19 May 2006, in final form 2 September 2006
Published 13 November 2006
Online at stacks.iop.org/JMM/16/2692

**Abstract**
A simple numerical approach based on the volume of fluid (VOF) method reveals that a 'W'-shaped, transient meniscus is ubiquitous during the formation of a uniformly curved meniscus within a microchannel, which has been believed to be dominant for the transients. The time that is needed to maintain the transient meniscus is correlated with viscosity, surface tension and geometry of the cavity. A generalized correlation is presented to predict the persistent time of the transient meniscus in a wettable microchannel (contact angle, $\theta < 90^\circ$) for Newtonian fluid.

## List of symbols

| | |
|---|---|
| $\theta$ | contact angle |
| $\rho$ | density |
| $t$ | time |
| $u_i$ | velocity vector |
| $x_i$ | coordinate component |
| $\sigma_{ij}$ | total stress tensor |
| $f_i$ | body force |
| $p$ | pressure |
| $\delta_{ij}$ | Kronecker delta tensor |
| $\eta$ | viscosity |
| $d_{ij}$ | strain rate tensor |
| $C$ | color function |
| $F$ | continuum surface force |
| $\gamma$ | surface tension coefficient |
| $\kappa$ | curvature |
| $[C]$ | jump of color function across the interface |
| $\vec{n}_s$ | unit free surface normal vector |
| $\vec{n}_w$ | unit normal vector directed into the wall |
| $\vec{t}_w$ | unit tangential vector directed into the fluid |
| $h_0$ | initial thickness of liquid film |
| $L$ | width of channel cavity |
| $S$ | spacing between the adjacent cavities |
| $h$ | meniscus height within the cavity |
| $t_r$ | effective relaxation time |
| $T_g$ | glass transition temperature |
| $\tau$ | dimensionless time |
| $y$ | dimensionless location |
| $\phi$ | aspect ratio of the cavity |
| $t_W$ | persistent time of the transient meniscus |
| $\alpha$ | proportionality constant |
| $k$ | universal constant for Newtonian fluid |

## 1. Introduction

When a stationary liquid film is in contact with a wettable channel or cavity, Laplace pressure is generated due to the wetting-induced curved interface, leading to the capillary movement of the liquid [1, 2]. This curvature-induced Laplace pressure is simply counterbalanced by the gravitational force (vertical capillary rise) or trapped air or defects in the void spaces (lateral capillary flow). Capillarity is important for studying micro/nanoscale patterning methods such as micromolding in capillaries (MIMIC) [3], nanoimprint lithography (NIL) [4] and capillary force lithography (CFL) [5]. In addition, most microfluidic devices utilize the movement of a fluid as an analyte or coolant, which necessitates fundamental understanding of the formation and shape of a meniscus at its early stage, in particular, as the channel size decreases to a few tens of nanometers [6, 7]. While capillarity has been studied extensively [8–10], capillarity in microchannels has not received much attention in spite of its importance in the above-mentioned systems. Much less is known about the evolution of transient meniscus in microchannels.

Recently, a 'W'-shaped, transient meniscus was observed prior to the formation of a uniformly curved meniscus when a polystyrene film was annealed within a cavity of the polydimethylsiloxane mold in conformal contact with the polymer surface [11]. Some speculation on the transient meniscus led us to consider that a certain time would be required for a viscous liquid to form a uniformly curved meniscus since the wall-induced perturbation needs to propagate toward the center of the channel. In this sense, it would be interesting to investigate how the transient meniscus evolves and how long it persists prior to the formation of a uniform curvature. Motivated by this question along with our earlier experimental observations, we performed a numerical analysis on the evolution of a meniscus inside a microchannel for Newtonian fluid. Although capillarity can either be found in capillary rise ($\theta < 90°$) or capillary depression ($\theta > 90°$), capillary rise is only considered in this study assuming that the same approach could be applied to capillary depression. As the capillary flow involves a moving free surface, a well-known continuum simulation strategy called the volume of fluid (VOF) method is used with the Eulerian grid system [12]. It is known that among the solution algorithms based on the Eulerian method, the VOF method is simple and efficient in dealing with complex flow patterns inside the cavity. Also, the continuum surface force (CSF) model is employed to consider the effects of surface tension and wall adhesion with the Eulerian grid system [13]. We further assume unsteady, incompressible flow and isothermal state of the system with slip boundary conditions.

## 2. Numerical method

According to mass and momentum balances, the governing equations of the two-dimensional system are given as follows:

$$\frac{\partial \rho}{\partial t} + \rho \frac{\partial u_i}{\partial x_i} = 0 \quad \text{(continuity equation)} \tag{1}$$

$$\rho \frac{\partial u_i}{\partial t} + \rho u_j \frac{\partial u_i}{\partial x_j} = \frac{\partial}{\partial x_j} \sigma_{ji}(u) + \rho f_i \quad \text{(Navier–Stokes equation)}, \tag{2}$$

where $\sigma_{ij} = -p\delta_{ij} + 2\eta d_{ij}$, $d_{ij} = \frac{1}{2}\left(\frac{\partial u_i}{\partial x_j} + \frac{\partial u_j}{\partial x_i}\right)$ ($i = 1, 2$ and $j = 1, 2$). Here $t$ is the time, $u_i$ is the velocity component in the $x_i$ direction, $\rho$ is the density, $\eta$ is the viscosity, $f_i$ is the body force component in the $x_i$ direction and $\sigma_{ij}$ and $d_{ij}$ denote the stress and the strain tensors, respectively. In the VOF method, the fractional volume is defined for element variable. The fractional volume is used to divide the total domain into two regions (occupied or empty). The values of the fractional volume in fully filled cells, partially filled cells and empty cells are given by unity, between zero and unity and zero, respectively. The fractional volume is then computed and updated at each time step following the advection equation,

$$\frac{\partial C}{\partial t} + u_i \frac{\partial C}{\partial x_i} = 0, \tag{3}$$

where $C$ is the color function (fractional volume). The process of free surface construction consists of three steps: first, the flow field is solved at one time step. Then the fluid volume flux from one element to the neighboring element is calculated [14]. Finally, the fractional volume is updated. This process for each time step is repeated until the desired time is reached.

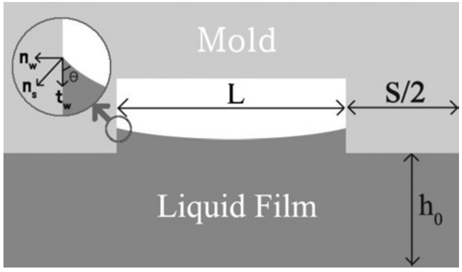


**Figure 1.** Illustration of the computational domain.

**Table 1.** Geometries considered in the simulation (see figure 1).

| Geometry | Case 1 | | Case 2 | | Case 3 | | Case 4 | |
|---|---|---|---|---|---|---|---|---|
| $L$ ($\mu$m) | 3 | 1.5 | 4 | 2 | 5 | 2.5 | 6 | 3 |
| $h_0$ ($\mu$m) | 0.5 | 0.25 | 0.5 | 0.25 | 0.5 | 0.25 | 0.5 | 0.25 |
| $S$ ($\mu$m) | 1.5 | 0.75 | 2 | 1 | 2.5 | 1.25 | 3 | 1.5 |

Much attention needs to be paid to deal with surface tension because of its dominant influence on flow pattern in micro/nanoscale. In order to consider the effect of surface tension in the Eulerian grid system, we used Brackbill's CSF model formulation [13], which converts the surface force to body force:

$$F = \frac{\gamma}{[C]} \kappa \nabla C, \qquad \kappa = -(\nabla \cdot n), \qquad n = \frac{\nabla C}{|\nabla C|}, \tag{4}$$

where $\gamma$ is the surface tension coefficient, $\kappa$ is the curvature and $[C]$ denotes the jump of $C$ across the interface. Finally, the boundary condition at the wall was imposed as the constant contact angle. This condition can be expressed using the unit free surface normal vector $\vec{n}_s$ along the wall,

$$\vec{n}_s = \vec{n}_w \cos\theta + \vec{t}_w \sin\theta, \tag{5}$$

where $\theta$ is the contact angle between the fluid and the wall, $\vec{n}_w$ is the unit normal vector directed into the wall and $\vec{t}_w$ is the unit tangential vector directed into the fluid.

The computation domain is shown in figure 1 where $h_0$ is the initial thickness of liquid film, $L$ is the width of channel cavity and $S$ is the spacing between the adjacent cavities. Four different geometries were considered in the simulation as described in table 1 where the aspect ratio defined as $L/h_0$ monotonically increases with two different cavity widths for the same aspect ratio. In this manner, the role of aspect ratio and channel width can be examined at the same time. The value of $S$ was determined such that the ratio of line width and spacing was maintained to be the same ($L/S = 2$). In addition to the geometrical parameters, material properties are also important. First, the density of liquid was set to be constant ($1.06 \times 10^3$ kg m$^{-3}$), which is independent of other parameters such as viscosity and surface tension. Second, a wide range of magnitudes were tested for surface tension and viscosity due to their significant impact on the transient behavior: 4–400 (mN m$^{-1}$) for surface tension and $10^{-3}$–$4 \times 10^9$ (Pa s$^{-1}$) for viscosity. While high-viscosity liquids such as polymer melt frequently show a shear thinning behavior, the viscosity could be assumed to be constant at extremely small shear rates as can be found in the capillary system presented here [15].

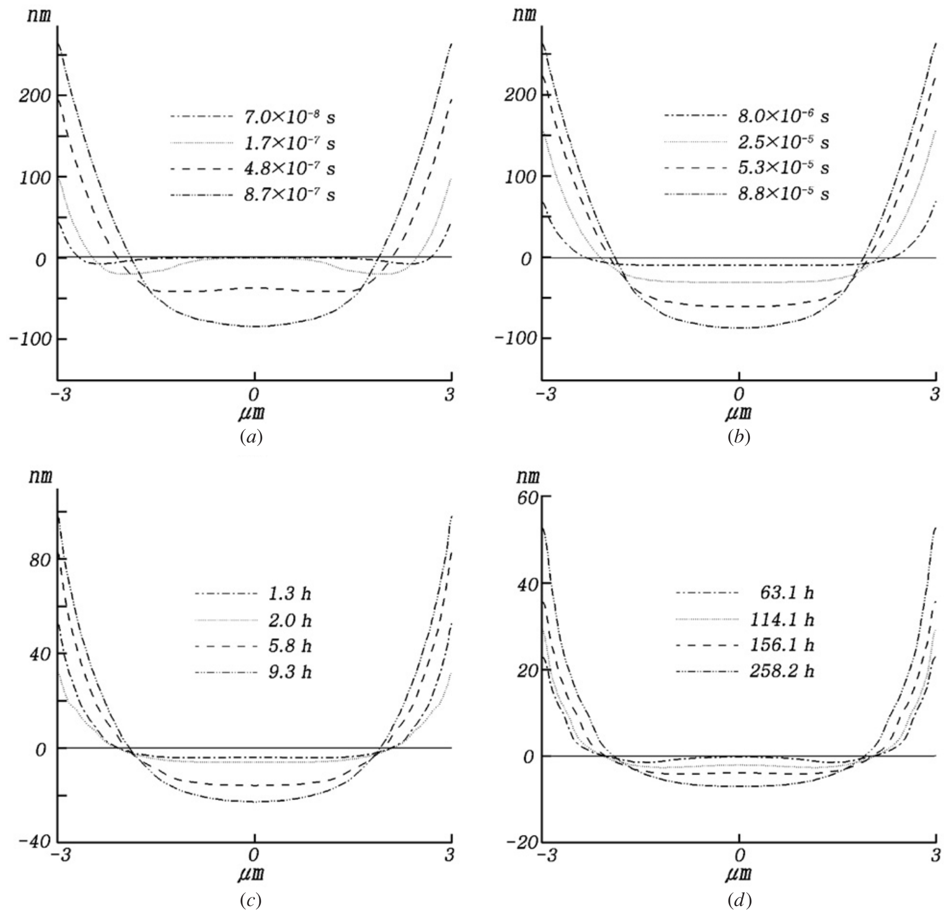


**Figure 2.** Typical numerical results for the evolution of the transient meniscus over time for four viscosities (increasing order): (*a*) $\eta = 1 \times 10^{-3}$ Pa s$^{-1}$, (*b*) $\eta = 1 \times 10^{-1}$ Pa s$^{-1}$, (*c*) $\eta = 5 \times 10^{7}$ Pa s$^{-1}$ and (*d*) $\eta = 4 \times 10^{9}$ Pa s$^{-1}$. Other parameters were set to be constant: $h_0 = 500$ nm, $\gamma = 40$ mN m$^{-1}$ and $L = 6\,\mu$m.

Finally, both surface tension and viscosity were assumed to be constant under isothermal conditions during the evolution of the transients.

## 3. Results and discussion

Typical numerical results for the transient meniscus are shown in figure 2 for a 6 $\mu$m channel. As can be seen from the figure, a flat or 'W'-shaped meniscus persists for a period of time prior to the formation of a 'U'-shaped, uniformly curved meniscus for different viscosities ranging from $10^{-3}$ to $10^{9}$ Pa s$^{-1}$. For a low viscosity liquid such as water (figure 2(*a*), $\eta = 1 \times 10^{-3}$ Pa s$^{2-1}$), the persistent time (defined as the time when the center point of meniscus is located at the lowest position) is merely on the order of $10^{-7}$ s, suggesting that it is unlikely to observe a transient meniscus under a simple optical setup. When the viscosity is increased by two orders of magnitude (figure 2(*b*)), the corresponding persistent time is increased roughly by two orders of magnitude. This linear relation can also be applied to a high-viscosity liquid or polymer melt (figures 2(*c*)–(*d*)) where the persistent time is on the order of hours to tens of hours [11]. In particular, the transient profiles shown in figure 2(*c*) have practical implications for the micromolding process involving polymer films such as NIL [4] and CFL [5]. For example, we previously observed in CFL that it took ∼30 min for a rubbery polymer to completely fill the cavity of the mold with a height of 600 nm and a width of 400 nm at 100 °C. The viscosity of the polymer was $\sim 10^{6}$ Pa s$^{-1}$ from the rheometrics spectroscopy (RMS) measurement at zero shear stress. If we assume a linear dependence of the persistent time on viscosity, the time scale for the evolution of meniscus at this viscosity is estimated to be several minutes. This time can be defined as an incubation time that is needed to form a uniform curvature prior to capillary rise of the polymer melt [5].

A physical interpretation is as follows: once the liquid wets the wall of a channel the perturbation propagates to the inside of the channel. During the propagation, the nearest region of the perturbation should be depressed to meet mass conservation. As a result, it follows that the transient meniscus first presents a W-shape and then evolves into a flat and finally a uniform curvature. The uniformly curved meniscus is a part of a circle, the radius of which is $(L/2)/\cos\theta$. This phenomenological explanation is not complete but can point out key aspects for the evolution of the transients. The time it takes for the film to form a uniform curvature strongly depended on viscosity, surface tension, film thickness and geometrical parameters. Of these, the effects of viscosity turned out to be dominant, which is readily understood in terms of mobility of the film. Interestingly, the whole evolution to form a uniform curvature takes approximately two to three times the persistent time as shown in figure 2.

To provide a dimensionless analysis for predicting the persistent time, we consider a simple one-dimensional conservation equation for a liquid film ($<10\ \mu$m) after reducing the original Navier–Stokes equation to a simple form [11, 16],

$$\eta \frac{\partial h}{\partial t} = -\frac{\gamma}{3} \frac{\partial}{\partial x}\left( h^3 \frac{\partial^3 h}{\partial x^3} \right), \tag{6}$$

where $h$ is the meniscus height within the cavity. To study the initial transients, it is sufficient to consider a linearized version of the equation:

$$\frac{\partial H}{\partial \tau} = -\frac{1}{3\phi^4} \frac{\partial^4 H}{\partial y^4}, \tag{7}$$

where $\phi \equiv L/h_0$ (the aspect ratio defined as the channel width divided by film thickness) and $\tau \equiv t/t_r$ ($t_r \equiv \eta h_0/\gamma$). Here, the height is scaled with respect to the initial film thickness $h_0$ for $H$, the time with respect to an effective 'relaxation' time $t_r$ for $\tau$, and the coordinate $x$ with respect to the channel width $L$ for $y$. $t_r$ can be viewed as an effective relaxation time since it can be interpreted as a time scale that is needed to form a uniform curvature within the channel. For example, in the case of polymer melt, the polymer chains are highly coiled and entangled so that it takes a lot of time for the chains to be relaxed. When we insert $\eta_0 \sim 6 \times 10^{10}$ Pa s$^{-1}$ at glass transition temperature ($T_g$) ($M_w = 1.4 \times 10^5$) [17], $h_0 = 1\ \mu$m, and $\gamma \sim 35$ mN m$^{-1}$ for polystyrene (PS) [18, 19], the relaxation time is calculated to be $\sim 1.7 \times 10^6$ s at $T_g$, indicating that it takes about 472 h or 20 days for the chains to be fully relaxed. In the case of water, on the other hand, the corresponding parameters are $\eta_0 \sim 9.3 \times 10^{-4}$ Pa s$^{-1}$ at 23 °C [1], $h_0 = 1\ \mu$m and $\gamma = 72$ mN m$^{-1}$ [1], yielding $t_r \sim 13$ ns.

The dimensionless version of mass balance shown in equation (7) indicates that the initial thickness profiles would be the same for the same dimensionless time ($\tau$), location ($y$) and geometry ($\phi$) [$H = H(\tau, y; \phi)$]. The functional dependence of the dimensionless channel width $y$ or channel width $L$ can be formulated into Laplace pressure ($\Delta P \sim \cos\theta \cdot \gamma/L$) since the rate of capillary rise at the wall, for example, would decrease with increasing channel width [20]. As a result, the persistent time of the transient meniscus ($t_W$) could be correlated with viscosity, aspect ratio and Laplace pressure, leading to

$$t_W = t_W(t_r, \phi, L) \approx t_W(\eta, L/h_0, \Delta P). \tag{8}$$

In figure 3($a$), we plotted $t_W$ as a function of $t_r$ for various geometrical conditions shown in table 1. As shown in the figure, $t_W$ is linearly proportional to $t_r$ for a given aspect ratio and Laplace pressure. Here, we define the proportionality constant as $\alpha(\phi, y)$, such that $t_W = \alpha(\phi, y) \cdot t_r$ following equation (8). The linear increase indicates that a high $t_r$ (low mobility) gives rise to sluggish movement of the liquid, thus requiring much time to form a uniform curvature. Furthermore, $\alpha(\phi, y)$ was found to increase with increasing aspect ratio. This is readily understood in terms of the propagation time and capillary movement of the liquid, corresponding to our earlier experimental observations using different channel widths for a given film thickness and $t_r$ [11]. Surprisingly, the measured persistent times did not show much

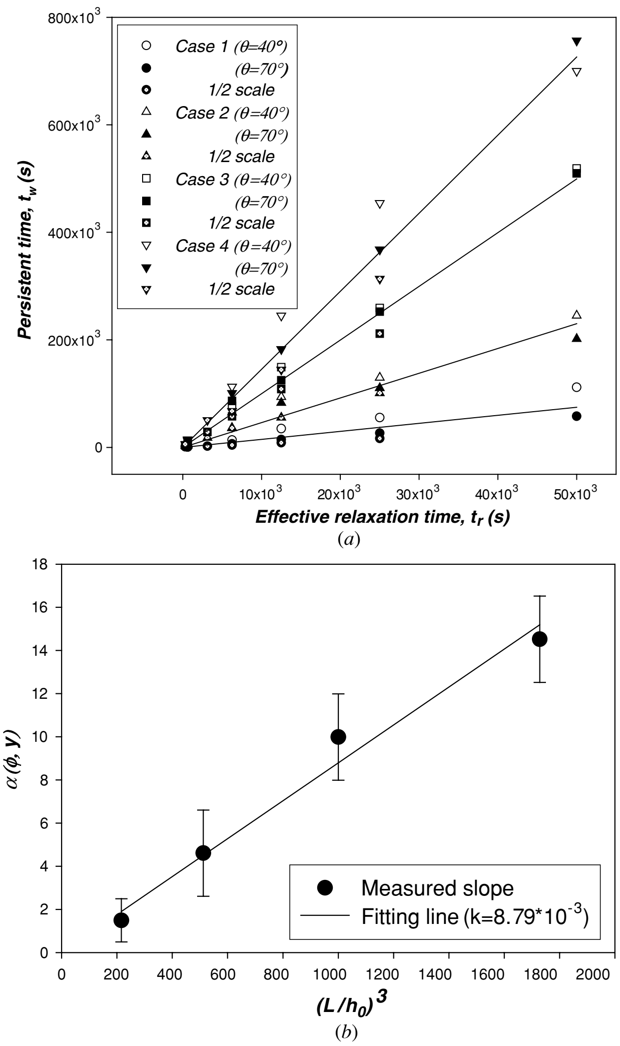


**Figure 3.** ($a$) Plot of the persistent time of the transient meniscus as a function of the effective relaxation time for various geometrical conditions shown in table 1 with two different contact angles (40° and 70°). For $\theta = 70°$, the data with the same aspect ratio but half the cavity width (1/2 scale) were also presented. ($b$) Plot of the proportionality constant in equation (9) as a function of the third order of aspect ratio.

difference for two contact angles (40° and 70°) and different cavity widths for a given $\phi$ and $t_r$. This finding implies that the persistent time might be independent of Laplace pressure or the propagation be mainly governed by material properties and cavity geometry, not by wetting kinetics at the wall. Also, this is supported by our earlier observation that the capillary rise takes place only after forming a uniformly curved meniscus [21]. Based on these findings, we propose a simple linear relation between $t_W$ and $t_r$:

$$t_W = \alpha(\phi, y) \cdot t_r \approx \alpha(\phi) \cdot t_r. \tag{9}$$

In figure 3($b$), we found that $\alpha(\phi)$ is best fitted with the third order of $\phi$, yielding the slope of $\sim 8.79 \times 10^{-3}$ from the regression. Thus, one can represent $t_W$ in terms of geometrical parameters and key material properties as follows:

$$t_W = k\frac{\eta L^3}{h_0^2 \gamma} \sim 8.79 \times 10^{-3} \phi^3 t_r, \tag{10}$$

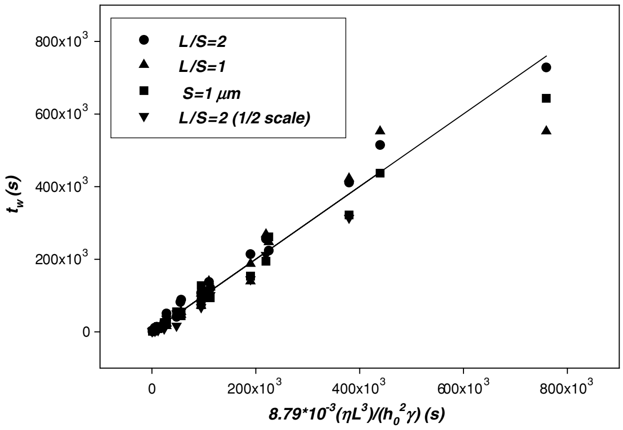


**Figure 4.** A generalized plot comparing the experimental data with the correlation presented in this study. Various geometrical conditions were tested for the plot including $L/S = 2$ and 1. For $L/S = 2$, the data with the same aspect ratio but half the cavity width (1/2 scale) were also presented. $S = 1$ $\mu$m indicates that the spacing was maintained constant with different values of $L$ shown in table 1.

where $k$ is the universal constant for Newtonian liquid films considered in this study. Figure 4 shows a generalized plot comparing the simulation data with the correlation derived in equation (10). A good agreement was seen for all the conditions tested except for relatively large scatterings for larger $t_W$. A question arises as to whether this generalized correlation can be applied to other geometries of the mold. As shown in figure 4, the influence of the spacing with respect to the cavity size seems non-significant for various mold geometries. This is because the meniscus formation appears to be governed by the movement of a liquid film within the cavity rather than mass transport from outside the cavity (the space region between cavities), which was observed experimentally in our previous work [21]. Thus, the correlation could be equally applied to different cavity sizes having different values of $L/S$.

## 4. Summary

We have presented numerical simulations on the evolution of the transient meniscus for a Newtonian liquid when a mold cavity is in contact with a liquid surface. A W-shaped meniscus was always found prior to the formation of a uniformly curved meniscus regardless of material properties (e.g., viscosity, surface tension, contact angle ($<90°$)) and geometry of the cavity (e.g., channel width, spacing, film thickness). Also a generalized correlation has been derived to predict the persistent time of the transient meniscus as a function of viscosity, surface tension and aspect ratio with an appropriate proportionality constant. It was found that the persistent time was independent of Laplace pressure and mainly governed by material properties and cavity geometry. Also, the whole evolution to form a uniform curvature took two to three times the persistent time for a given liquid film. The generalized correlation was also in good agreement with various mold geometries, suggesting that it is potentially widely applicable to describing wetting behavior in a wettable microchannel or flow kinetics in micro/nanofluidics.

## Acknowledgments

This research was supported by the Center for Nanoscale Mechatronics & Manufacturing (06K1401-01020), one of the 21st Century Frontier Research Programs by the Ministry of Science and Technology, and supported in part by the Nanoscopia Center of Excellence at Hanyang University and the Micro Thermal System Research Center of Seoul National University.

## References


[1] Adamson A W and Gast A P 1997 *Physical Chemistry of Surfaces* (New York: Wiley)

[2] Rowlinson J S 1984 *Molecular Theory of Capillarity* (New York: Oxford University Press)

[3] Kim E, Xia Y N and Whitesides G M 1995 Polymer microstructures formed by molding in capillaries *Nature* **376** 581–84

[4] Chou S Y, Krauss P R and Renstrom P J 1996 Imprint lithography with 25-nanometer resolution *Science* **272** 85–87

[5] Suh K Y, Kim Y S and Lee H H 2001 Capillary force lithography *Adv. Mater.* **13** 1386–89

[6] Stone H A, Stroock A D and Ajdari A 2004 Engineering flows in small devices: microfluidics toward a lab-on-a-chip *Annu. Rev. Fluid. Mech.* **36** 381–411

[7] Tas N R, Haneveld J, Jansen H V, Elwenspoek M and Van Den Berg A 2004 Capillary filling speed of water in nanochannels *Appl. Phys. Lett.* **85** 3274–76

[8] Gao C 1997 Theory of menisci and its applications *Appl. Phys. Lett.* **71** 1801–03

[9] Chen Y F, Weng J G, Lukes J R, Majumdar A and Tien C L 2001 Molecular dynamics simulation of the meniscus formation between two surfaces *Appl. Phys. Lett.* **79** 1267–69

[10] Yang L J, Yao T J and Tai Y C 2004 The marching velocity of the capillary meniscus in a microchannel *J. Micromech. Microeng.* **14** 220–25

[11] Suh K Y, Chu S and Lee H H 2004 W-shaped meniscus from thin polymer films in microchannels *J. Micromech. Microeng.* **14** 1185–89

[12] Hirt C W and Nichols B D 1981 Volume of fluid (VOF) method for the dynamics of free boundaries *J. Comput. Phys.* **39** 201–25

[13] Brackbill J U, Kothe D B and Zemach C 1992 A continuum methods for modeling surface tension *J. Comput. Phys.* **100** 335–54

[14] Park J S, Kim S M, Kim M S and Lee W I 2005 Finite element analysis of flow and heat transfer with moving free surface using fixed grid system *Int. J. Comput. Fluid* D **19** 263–76

[15] Ferry J D 1980 *Viscoelastic Properties of Polymers* (New York: Wiley)

[16] Oron A, Davis S H and Bankoff S G 1997 Long-scale evolution of thin liquid films *Rev. Mod. Phys.* **69** 931–80

[17] Bicerano J 1996 *Prediction of Polymer Properties* (New York: Marcel Dekker)

[18] Wu S 1970 Surface and interfacial tensions of polymer melts. II. Poly(methyl methacrylate), poly(n-butyl methacrylate), and polystyrene *J. Phys. Chem.* **74** 632–38

[19] Wu S 1971 Calculation of interfacial tension in polymer systems *J. Polym. Sci.* **34** 19–30

[20] Suh K Y, Kim P and Lee H H 2004 Capillary kinetics of thin polymer films in permeable microcavities *Appl. Phys. Lett.* **85** 4019–21

[21] Suh K Y, Yoo P J and Lee H H 2002 Meniscus formation and breakdown of thin polymer films in microchannels *Macromolecules* **35** 4414–18